Global sea-salt modeling: Results and validation against multicampaign shipboard measurements

Marcin L. Witek,[1,2] Piotr J. Flatau,[3] Patricia K. Quinn,[4] and Douglas L. Westphal[5]

[1] Open-ocean measurements of sea-salt concentrations from five different campaigns are used to validate the sea-salt parameterization in numerical models. The data set is unique in that it is from open-ocean shipboard measurements which alleviates typical problems associated with onshore wave breaking on land stations (surf zone). The validity of the sea-salt parameterizations is tested by employing a global forecasting model and transport model with detailed representation of dry and wet deposition, advection and diffusion, and other physical processes. It is shown that the inclusion of these processes leads to good agreement with shipboard measurements. The correlation coefficient of measured and modeled sea-salt mass concentrations for all data points was 0.76 and varied from 0.55 to 0.84 for different experiments. Average sea-salt mass concentration was 4.6 $\mu g/m^3$ from measurements and 7.3 $\mu g/m^3$ from the model, for all considered experiments. It was found that model-measurements discrepancies were affected by wet deposition uncertainties but also suggested was the influence of source uncertainties in the strong wind-speed regime, lack of a wind-speed threshold for emission onset, and lack of size differentiation in applied deposition velocity. No apparent relationship between the water temperature and the measured sea-salt concentration was found in the analyzed data set.

1. Introduction

[2] Sea-salt aerosol is a very important component of the atmospheric aerosol. It exerts a strong influence on radiation, cloud formation, meteorology, and chemistry of the marine atmosphere [*Lewis and Schwartz*, 2004]. An accurate understanding of these influences is essential to modeling climate and climate changes. It is considered to be one of the major contributors to the total particulate matter present in the atmosphere with estimates of the annual emission varying from 0.3×10^{12} to 30×10^{12} kg [*Lewis and Schwartz*, 2004].

[3] During recent years, there were many attempts to improve the prediction of the atmospheric sea-salt aerosol. Some of this effort was centered on refinements of the sea-salt emission function. Initial studies of *Monahan et al.* [1986] and *Smith et al.* [1993] were further improved and evaluated by *Andreas* [1998], *Hoppel et al.* [2002], *Gong* [2003], and other investigators [cf. *Lewis and Schwartz*, 2004]. Other measurement methods and parameterization approaches were developed by *Reid et al.* [2001], who exploited aircraft measurements in a concentration buildup method, and *Petelski et al.* [2005], who performed sea-salt concentration gradient measurements in the Baltic Sea and developed a sea-salt emission parameterization based on the surface wind speed and significant wave height. Accompanying studies of whitecap coverage [*Zhao and Toba*, 2001; *Stramska and Petelski*, 2003] resulted in improvements of emission parameterizations based on the whitecap method.

[4] Some of the recent effort has focused on global sea-salt modeling and air quality studies. The influence of the source formulation on modeling of the global sea-salt distribution was investigated by *Guelle et al.* [2001]. *Grini et al.* [2002], *Gong et al.* [2002], and *Takemura et al.* [2000] investigated the global sea-salt budget, annual cycle, and sea-salt radiative impact, employing sophisticated multibin sectional aerosol transport models. However, most of these numerical efforts were focused on describing large-scale characteristics, either spatial or temporal. Typically, validations of monthly averaged observations at selected locations were performed, and often modelers did not consider properly the size limits of measured particles and the techniques used for measuring the mass concentration [*Guelle et al.*, 2001; *Grini et al.*, 2002; *Gong et al.*, 2002]. Often the accuracy of presented simulations was limited by coarse horizontal resolution, typical for general circulation models.

[5] In this work, we employ high temporal and spatial resolution ship measurements to validate the sea-salt emission source function and performance of a global aerosol

---

[1]Interdisciplinary Centre of Mathematical and Computational Modeling, University of Warsaw, Warsaw, Poland.
[2]Institute of Geophysics, University of Warsaw, Warsaw, Poland.
[3]Scripps Institution of Oceanography, University of California, San Diego, La Jolla, California, USA.
[4]Pacific Marine Environmental Laboratory, National Oceanic & Atmospheric Administration, Seattle, Washington, USA.
[5]Marine Meteorology Division, Naval Research Laboratory, Monterey, California, USA.

transport model. We begin with comprehensive description of the models and the sea-salt emission source function that was implemented. Next, we discuss experimental techniques that were employed by the National Oceanic and Atmospheric Administration's (NOAA) Pacific Marine Environmental Laboratory (PMEL) to measure sea-salt mass concentrations during five field projects, Aerosols99, INDOEX, Aerosol Characterization Experiment (ACE-Asia), New England Air Quality Study (NEAQS)-2002, and NEAQS-2004. Measured sea-salt concentrations are compared with model predictions, together with accompanying analysis of surface wind speed and precipitation obtained from measurements and the model. Finally, we synthesize all the experimental analyses, investigate average characteristics, and discuss sources of uncertainties.

2. Implementation of Sea Salt in the Model

[6] We use the current version of the Navy Aerosol Analysis and Prediction System (NAAPS) model, which contains five species, gaseous SO_2, particulate sulfates (SO_4), mineral dust, smoke/soot, and sea-salt aerosol. All these species are treated as passive tracers, not reacting with each other, with the exception of gaseous SO_2, which can be transformed to particulate sulfates. Physical processes that apply to each species include the following: (1) emission from the surface, (2) dispersion and advection by the wind, and (3) removal from the atmosphere by wet and dry deposition. The same processes are considered in the case of sea salt. To accomplish the validation part of our research, we performed rerun of the model. We used the global circulation model Navy Operational Global Atmospheric Prediction System (NOGAPS) [Hogan and Rosmond, 1991] to provide input meteorological fields to drive the tracer transport model and analyzed 7 years of data which encompass the study period.

2.1. Models Description

[7] In this study, we use results from the NAAPS model, which was developed in the Naval Research Laboratory in Monterey, USA. NAAPS is a global three-dimensional aerosol and air pollution model, based primarily on the Danish Eulerian Hemispheric Model (DEHM) [Christensen, 1997]. Many modifications, however, were applied to the original DEHM model, before it became the operational, real-time forecast system for the Naval Research Laboratory. The following description of the model is partially based on Christensen's [1997] paper, with the special emphasis on the processes relevant to the sea-salt prediction.

[8] The set of equations solved in the model has the form:

$$\frac{\partial q_i}{\partial t} = -\left(u\frac{\partial q_i}{\partial x} + v\frac{\partial q_i}{\partial y} + \varsigma\frac{\partial q_i}{\partial \sigma}\right)$$
$$+ \left(K_x\frac{\partial q_i}{\partial x^2} + K_y\frac{\partial q_i}{\partial y^2} + \frac{\partial\left(\Gamma^2 K_z\frac{\partial q_i}{\partial \sigma}\right)}{\partial \sigma}\right) + P_i - Q_I,$$
$$i = 1, nq \tag{1}$$

where q_i is the mass mixing ration for the specie i: $q_i = c_i/\rho$, where c_i is the mass concentration and ρ is the density of air,

x and y are the horizontal coordinates and σ is the terrain-following vertical coordinate ($\sigma = p/p_s$, where p is the present pressure and p_s surface pressure), u and v are horizontal velocities and ς is the vertical velocity in σ coordinates. K_x and K_y are the horizontal diffusion coefficients (assumed to be constant: $K_x = K_y = 6 \times 10^4$ m^2 s^{-1}), and K_z is the vertical diffusion coefficient, which will be described further on. $\Gamma = d\sigma/dz$, and assuming hydrostatic equilibrium and introducing the ideal gas law $\Gamma = -g\ p/p_s = -g\sigma/RT$, where g is acceleration due to gravity, R is the gas constant (for ambient air), and T is the temperature. P_i and Q_i are the production and loss terms for modeled species. nq is the number of species in the model.

[9] The boundary condition at the ground is represented by the mass fluxes due to dry deposition and the surface emission: $K_\sigma\frac{\partial q_i}{\partial \sigma} = -\Gamma v_d q_i + \frac{G}{\sigma}E_s$, where v_d (m/s) is the dry deposition velocity, and E_s (g/m^2 s) is the surface emission. Free boundary conditions are applied at the top layer.

[10] The vertical diffusion coefficient parameterization K_z is based on the Monin-Obukhov similarity theory for the surface layer. The K_z profile is extended to the whole boundary layer by using a simple extrapolation [Hertel et al., 1995]

$$K_z = \max\left(\frac{\kappa u_* z}{\phi(z/\nu L)}\left(1 - \frac{z}{z_{mix}}\right), 0.1\,\text{m}^2\text{s}^{-1}\right),$$

where $\phi(z/L)$ is the similarity function for heat, κ is the von Karman constant, u_* is the friction velocity, z is the height above the surface, z_{mix} is the height of the mixing layer, and L is the Monin-Obukhov length.

[11] The mixing layer height z_{mix} is calculated by a simple parameterization based on an energy balance equation for the internal boundary layer [e.g., Gryning and Batchvarova, 1990]

$$\left(N^2 z_{mix} + 1.9\frac{u_*^2}{z_{mix}}\right)\left(\frac{\partial z_{mix}}{\partial t} + u\frac{\partial z_{mix}}{\partial x} + v\frac{\partial z_{mix}}{\partial y} + w\right)$$
$$= \frac{w_*^3}{z_{mix}} + \frac{1.25u_*^3}{z_{mix}} - \frac{u_*^2}{\tau} - \frac{w_*^2}{2\tau},$$

where N is the Brunt-Vaisala frequency, $N^2 = \gamma\ g\ /\ T$ (γ is the lapse rate and T is the temperature), w is the vertical velocity at z_{mix}, $w_* = (g\ /\ T\cdot\max(H_{sen}/\rho c_p, 0)\cdot z_{mix})^{1/3}$ is the turbulent velocity scale, and τ is the dissipation timescale (= 1000 s). The effect of entrainment is ignored in the above balance equation.

[12] The dry deposition of sea-salt particles is treated in a very simplified manner. Dry fluxes are equal to the mass concentration in the lower level times a dry deposition velocity which is differently defined for the open water surface and for all other types of surfaces. The dry deposition velocity to open water is given by the formula in the work by Slinn and Slinn [1980] assuming a dry mass mean radius near 1 μm $v_d \cong u_*^2/U_{10} = C_d U_{10}$, where U_{10} is the wind velocity at 10 m above the sea surface and $C_d \approx 1.3 \times 10^{-3}$ is the drag coefficient.

[13] Over non-open water surfaces the dry deposition velocity is based on the formulation by *Walcek et al.* [1986]

$$v_d = \begin{cases} \dfrac{u_*}{a}\left(1 + \left(\dfrac{-300}{L}\right)^{2/\nu3}\right) & for\ L < 0 \\[2mm] \dfrac{u_*}{a} & for\ L > 0 \end{cases},$$

where $a = 500$ (except for a forest with leaves, where $a = 100$), and L is the Monin-Obukhov length. The choice of the above deposition velocities is arbitrary, and these parameterizations will be improved as size differentiation is introduced to the model.

[14] The wet deposition of sea-salt particles is assumed to be similar to the sulfate aerosol and is based on a simple scavenging ratio formulation [see, e.g., *Inversen*, 1989]. The scavenging coefficient W (s^{-1}) at a given σ level is given as

$$W(\sigma) = \begin{cases} \dfrac{\Lambda_{bc}}{H}\dfrac{P_a(\sigma)}{\rho_w} & below\ cloud\ scavenging \\[2mm] \dfrac{\Lambda_c}{H}\dfrac{P(\sigma)}{\rho_w} & in\ cloud\ scavenging \end{cases},$$

where $P_a(\sigma)$ and $P(\sigma)$ $(kg\ m^{-2}\ s^{-1})$ are the total downward flux densities of precipitation mass at a given σ level below or in a precipitating cloud, respectively. H is an effective thickness for scavenging (set to 1000 m), $\Lambda_{bc} = 1 \times 10^5$ is the below-cloud scavenging ratio, $\Lambda_c = 7 \times 10^5$ is the in-cloud scavenging ratio, and ρ_w is the density of water. The condensation scheme is the same as in NOGAPS atmospheric model and is further described in the work of *Hogan and Rosmond* [1991].

[15] Equation (1) is solved on the spherical Gaussian grid with horizontal resolution $1° \times 1°$ and 24 vertical irregular σ-coordinate levels. The average depth of the first layer is around 34 m, and consecutive layers gradually increase in depth toward the top layer, which ends at around 18 km. The time integration is performed by splitting equation (1) into several submodules, (1) three-dimensional advection, (2) vertical diffusion coupled with emission and dry deposition, and (3) horizontal diffusion.

[16] The three-dimensional advection is solved by a semi-Lagrangian algorithm [*Staniforth and Cote*, 1991; *Ritchie*, 1987]. A one-dimensional algorithm that is implicit in time and has a finite element space discretization is used for the horizontal and vertical diffusion equations. The integration time step in operational NAAPS performance is half an hour for vertical diffusion and 1 hour for all other processes, whereas in simulations performed in this study, it was 15 min for vertical diffusion and 30 min for other processes.

[17] The NAAPS model is driven by meteorological fields obtained from NOGAPS [*Hogan and Rosmond*, 1991]. Although current operational NOGAPS resolution is $0.5 \times 0.5°$, the simulation performed in this study was based on the coarser $1 \times 1°$ resolution. NOGAPS analyses are available every 6 h (at 00, 06, 12, and 18 coordinated universal time).

2.2. The Sea-Salt Emission

[18] The most commonly used formulations of the size-dependent source functions are those of *Monahan et al.*

[1986] and *Smith et al.* [1993]. Monahan based his equation on measurements of the size-resolved sea-salt number concentration over laboratory-generated whitecaps. His expression is valid for particles with radius from 0.8 to 8 μm at a relative humidity (RH) of 80%. The formulation of Smith et al. is based on a steady state dry deposition method, which is valid for particles with radii greater than about 5 microns at 80% RH [*Lewis and Schwartz*, 2004; *Hoppel et al.*, 2002]. Such particles are mostly larger jet drops and spume drops, and their residence time in the atmosphere is much shorter than for particles with smaller radii, because of the greater dry deposition and gravitational fallout.

[19] In NAAPS, the sea-salt dry mass flux from the surface is given by the equation $F = 1.37 \times 10^{-13}U_{10}^{3.41} \left[\frac{kg}{m^2 s}\right]$, where U_{10} is the wind speed at 10 m above the sea surface. This formulation of the source function is based on the whitecap method and the Monahan's formulation of the source function.

3. Experimental Methods

[20] Concentrations of ambient air chemical components in the submicron and supermicron size ranges were determined by the NOAA's PMEL. Aerosol particles were sampled 18 m above the sea surface through a heated mast that extended 5 m above the aerosol measurement container. The mast was capped with a horizontal inlet nozzle that was rotated into the relative wind to maintain nominally isokinetic flow and minimize the loss of supermicron particles. Air entered the inlet through a 5-cm diameter hole, passed through a 7-degree expansion cone, and then into the 20-cm inner diameter sampling mast. The flow through the mast was 1 m^3 min^{-1}. Wind tunnel tests have shown that the transmission efficiency for particles with aerodynamic diameters less than 6.5 μm (the larger size tested in wind tunnels) is greater than 95% [*Bates et al.*, 2002]. For particles in the 6.5- to 10-μm size range, for which collection efficiency is expected to decrease, there may have been a loss in sea-salt mass of up to 10%.

[21] The lower part of the mast was heated to establish a stable reference RH equal to $55 \pm 5\%$. A stable reference RH allowed for constant instrumental size segregation in spite of varying ambient RH. Two-stage multijet cascade impactors [*Berner et al.*, 1979] was used at the lower end of the mast to collect atmospheric particles. Aerodynamic cutoff diameters were 1.1 and 10 μm for submicron and supermicron size ranges, respectively, with the segregation at 55% RH. Sampling periods ranged from 4 to 6 h. Ion chromatography method [*Quinn et al.*, 1998] was used to specify chemical composition of collected aerosol samples. The analyzed components include sea salt, sulfate, nitrate, total organic carbon, elemental carbon, and mineral dust. Methodology of the chemical analysis is described in the papers by *Quinn et al.* [2001, 2002].

[22] Non−sea salt sulfate concentrations were calculated from Na^+ concentrations and the ratio of sulfate to sodium in seawater. Sea-salt aerosol concentrations were calculated as sea salt $(\mu g/m^3) = Cl^-(\mu g/m^3) + Na^+(\mu g/m^3) \times 1.47$, where 1.47 is the seawater ratio of $(Na^+ + K^+ + Mg^{+2} + Ca^{+2} + SO_4^- + HCO_3^-)/Na^+$ [*Holland*, 1978]. This approach prevents the inclusion of non−sea salt K^+, Mg^{+2}, Ca^{+2}, SO_4^-,
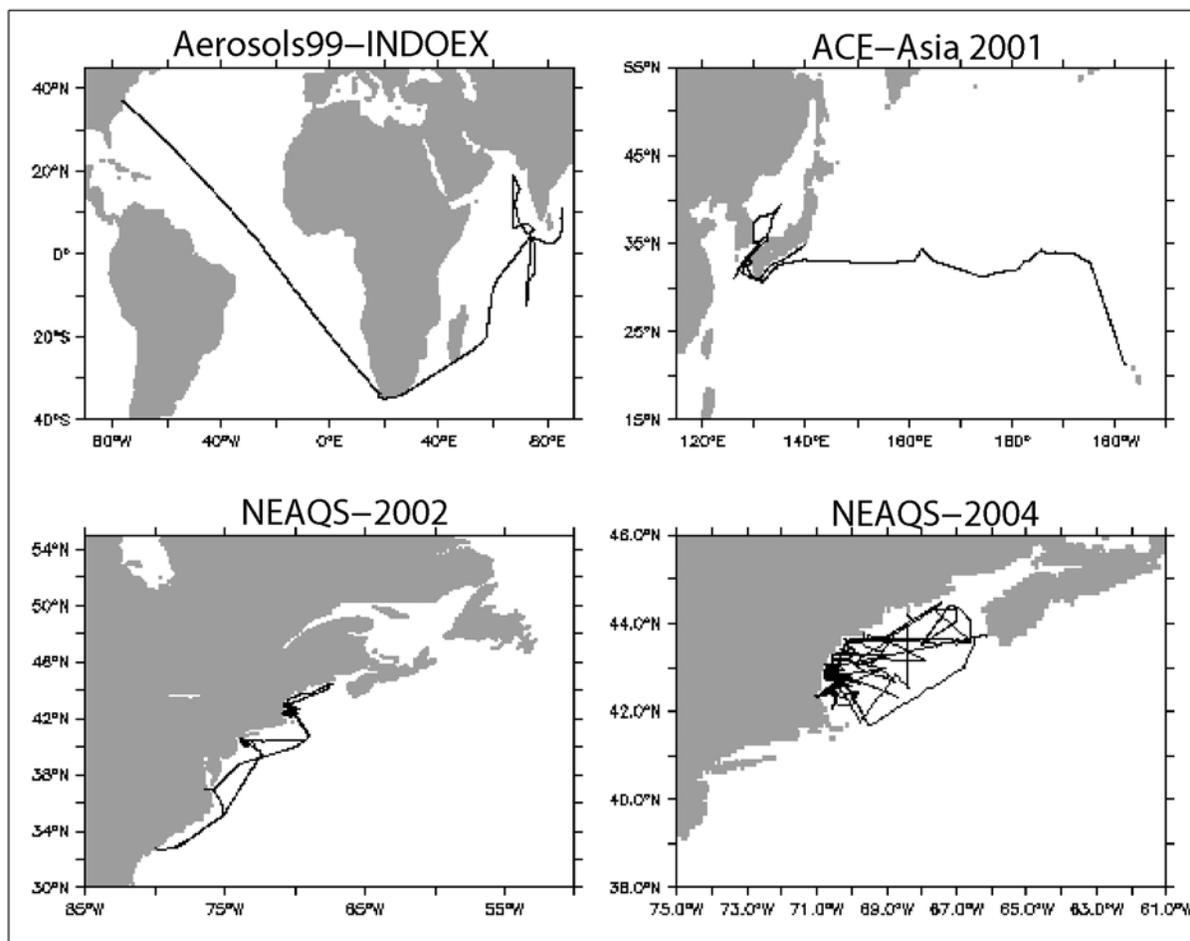
Figure 1. Maps and corresponding ship tracks (black lines) during the four PMEL Atmospheric Chemistry Group experiments: Aerosols99-INDOEX, ACE-Asia, NEAQS-2002, and NEAQS-2004.

and HCO_3^- in the sea-salt mass and allows for the loss of Cl^- mass through Cl^- depletion processes. It also assumes that all measured Na^+ and Cl^- is derived from seawater.

[23] The equation that was used to derive sea-salt mass concentrations explicitly includes the Cl^- concentration instead of assuming a Cl^- concentration based on the Na/Cl ratio in seawater. If the Na/Cl ratio and measured Na are used to determine the sea-salt concentration, the sea-salt concentration may be overestimated as the amount of Cl that is lost by replacement with SO_4 will not be taken into account. Since the measured Cl concentration was used, the amount of Cl that is lost by replacement with other acids were taken into account.

[24] The upper limit for the supermicron size range, which is defined by the particle aerodynamic radius 5 μm at 55% RH, corresponds almost exactly to the size limit for modeled sea-salt particles, which is 4 μm dry radius. Therefore the total measured sea-salt mass and mass modeled with NAAPS reflect the same size range, allowing for direct comparisons.

[25] Additional measurements made abroad the ship include wind speed, wind direction, rainfall rate, water temperature, and water salinity. True wind speed and direction were calculated from measurements obtained with the Ships IMET wind sensor. The sensor was mounted 14 m above the sea surface. The true North and East components of the wind vector were calculated and then averaged into 15-min intervals. The true wind vector was calculated from these components and is given as wind speed and wind direction in compass degrees. The measured wind speed, additionally averaged over 6 h encompassing the time of model output, was compared with the wind speed from the model at 10 m above the sea surface. The rainfall rate was measured with a Scientific Technology Inc. ORG-100 Optical Precipitation Intensity Sensor. The 15-min averaged data are reported in units of mm/hr. The rain rate was compared with the rate of the sea-salt wet deposition inferred from the model, given in milligrams per square meter per 6 h. The sea surface temperature and salinity were measured with the ship's online Sea-Bird thermosalinograph. The inlet for the sample water into the thermosalinograph was near the bow at approximately 4-m depth.

4. Results: Comparison With the Observational Data

[26] In this study, we analyzed data from five field campaigns conducted by the PMEL Atmospheric Chemistry
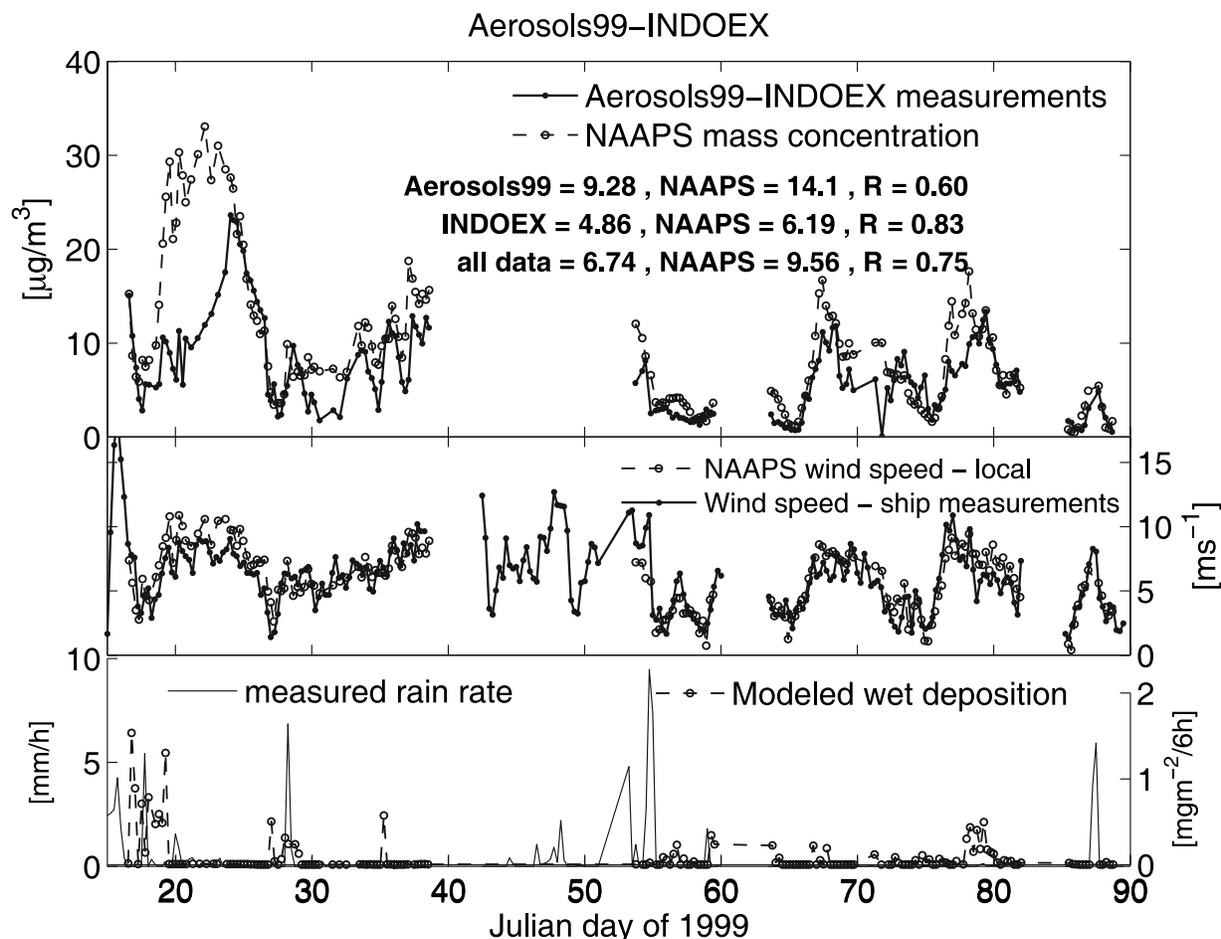
Figure 2. Top panel, comparison of the model concentrations with measurements during Aerosols99-INDOEX experiment; middle panel, measured and NAAPS-modeled wind velocity during the cruise; lower panel, the rain rate measured from the ship (left axis) and the rate of sea-salt wet deposition in the model (right axis).

Group. Maps of the regions together with corresponding ship tracks are presented in Figure 1.

4.1. Aerosols99-INDOEX Experiment

[27] This project was conducted in the January to March 1999 timeframe. NOAA R/V Ronald H. Brown, equipped with the PMEL facility, sailed from Norfolk, Virginia to Male, Maldives via Cape Town in South Africa and Mauritius in the South Indian Ocean. The first part of the experiment, while the ship headed from the Eastern Coast of the US toward the Indian Ocean was named Aerosols99, while its main part, after departing Mauritius and exploring the Indian Ocean, was named INDOEX.

[28] Figure 2 (upper panel) presents comparisons between measurements and NAAPS modeled sea-salt mass concentrations during the Aerosols99 and the INDOEX experiments. The middle panel presents surface wind velocities during the cruise measured from the ship and those predicted by the model. Lower panel shows rain rate (left axis) as observed from the ship and the rate of sea-salt wet deposition in the model (right axis).

[29] There is a good agreement between two data sets presented in the upper panel of Figure 2, as indicated by the high correlation coefficient equal to 0.75 for all data points.

Average values from the model and measurements agree within 48 and 73% in the case of Aerosols99 and INDOEX, respectively, indicating that NAAPS reproduces well the sea-salt concentrations measured at the surface. There are, however, instances where the model overestimates measured concentrations.

[30] In particular, model concentrations are too large for the period between days 18 and 25. During this period, concentrations over 20 $\mu g/m^3$ were measured, but no strong winds were observed. Prior to this high loading episode, there was no observed rainfall that could have accounted for the sea-salt removal and decreased surface concentrations. There is also no evidence of increased surface wind velocity in the region up to 150 km around the ship. *Bates et al.* [2001] suggested the influence of the marine boundary layer (MBL) height on observed sea-salt concentration increase on day 25. Radiosonde measurements [see *Bates et al.*, 2001] of RH indicated that the MBL decreased to 1.3 km on day 25, whereas before that date, MBL ranged from 2.0 to 2.5 km. Reduced vertical mixing because of lower MBL height, under relatively similar emission conditions, would result in increased aerosol concentrations. Such dependence is expected for aerosols that are well mixed within the boundary layer, which can be coarsely assumed for mea-
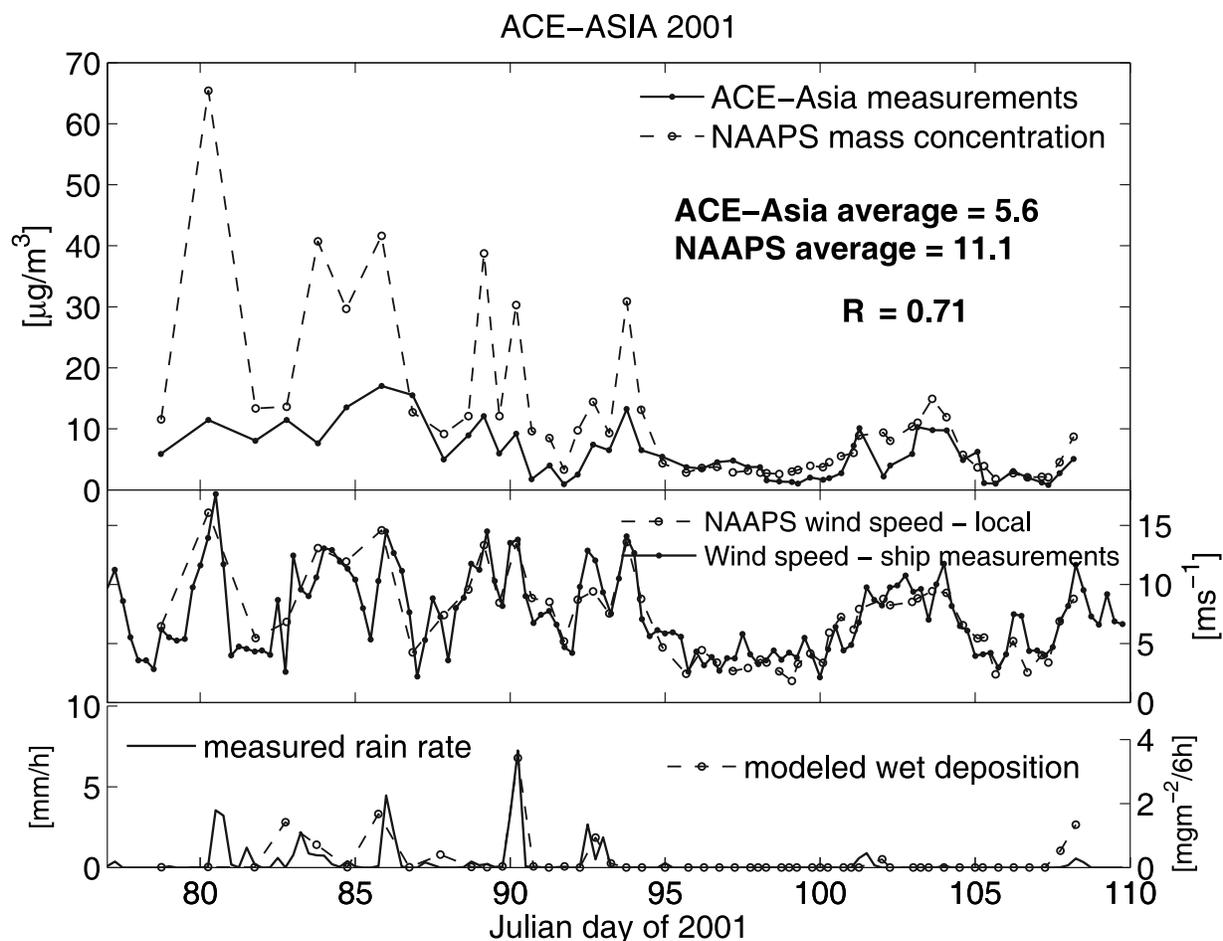
Figure 3. Top panel, comparison of the model-predicted concentrations with the measurements during the ACE-Asia experiment; middle panel, measured and NAAPS-modeled wind speed during the cruise; lower panel, the rain rate measured from the ship (left axis) and the rate of sea-salt wet deposition in the model (right axis).

sured and modeled particles considered in this paper. An independent study of *Park et al.* [1990] showed such dependence, but they also noted that the relation between aerosol concentrations and mixing height depends also on wind speed or atmospheric stability, and this can affect both the dilution of particles already present in MBL and the production and subsequent entrainment of the aerosol particles upward. On the other hand, model predictions of the MBL height did not show substantial reduction in comparison to that observed from radiosondes. This could explain why the modeled concentrations were relatively constant.

4.2. ACE-Asia Experiment

[31] The ACE-Asia was conducted in March and April of 2001 in the Western Pacific region. NOAA research ship R/V Ronald H. Brown sailed from Hawaii to the Japan Sea performing a number of radiation and chemical measurements on board. Figure 3, upper panel, presents comparisons of measurements from the ship with the NAAPS sea-salt mass concentrations during the cruise. The middle panel shows time trends of measured and modeled surface wind velocities, and the bottom panel presents rain rate measurements (left axis) and modeled rate of sea-salt wet deposition (right axis).

[32] For the entire experiment, the average NAAPS sea-salt mass concentration is almost two times higher than the measured one. In particular, NAAPS overestimates the measured concentrations between days 79 and 95 when the ship sailed over the open ocean. On the contrary, near the shore and in the Sea of Japan, model predictions show much better agreement with the measurements.

[33] Surface wind speed and deposition processes have to be considered to investigate the open-ocean discrepancy. Between days 79 and 95, the ship encountered the passage of several frontal systems with intense storms and very strong surface winds. On day 81, the measured wind velocity, averaged over 6 h, reached 18 m/s. The measured average for this open-ocean period is 8.9 m/s, almost twice as high as the wind speeds during the INDOEX and NEAQS experiments (see Table 2). A reasonable explanation for too high model concentrations might be related to weaknesses of the source function formulation, especially for strong surface winds. The emission function, being proportional to wind speed to the power 3.41, is accurate for calm and moderate conditions, but might fail in windy conditions, overpredicting emitted mass [*Andreas*, 1998].
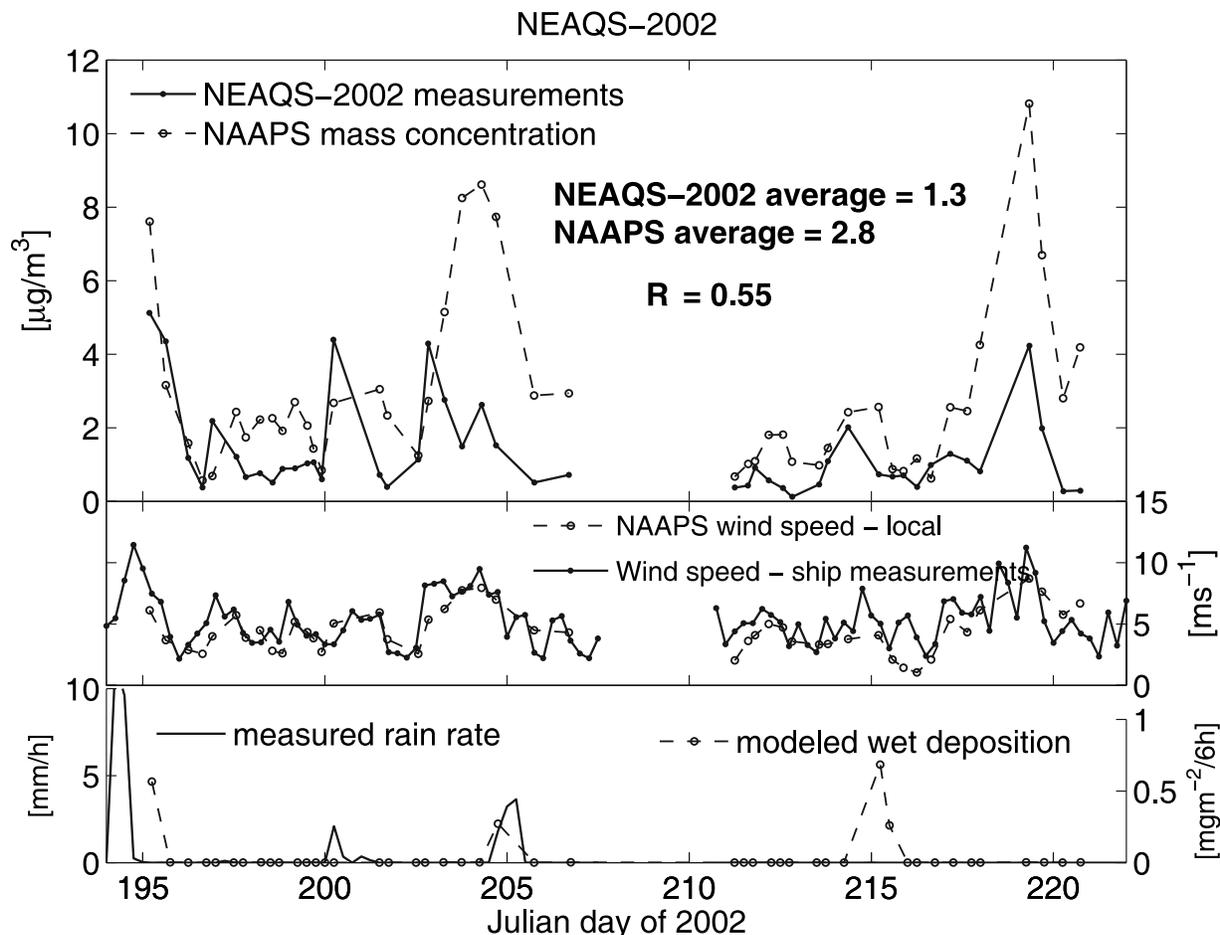
Figure 4. Top panel, comparison of the model concentrations with the measurements during the NEAQS-2002 experiment; middle panel, measured and NAAPS modeled wind speed during the cruise; lower panel, rain rate measured from the ship (left axis) and rate of sea-salt wet deposition in the model (right axis).

[34] Wet deposition processes may also contribute to observed discrepancies. Ship measurements of rain rate indicate the presence of persistent but mostly small magnitude rainfalls during the open-ocean period, with several more intense downpours associated with the frontal passages. Not all of these precipitation events were captured by NOGAPS, therefore affecting the magnitude of wet deposition.

4.3. NEAQS-2002 Experiment

[35] The NEAQS-2002 was a multi-institutional research project focusing on the understanding of the atmospheric processes that control production and distribution of air pollutants in the New England region. It took place in July and August of 2002. The NOAA ship R/V Ronald H. Brown was deployed into the Gulf of Maine and surrounding waters with a complete set of chemical and meteorological sensors to track the transport and transformation of air pollution. Figure 4 presents a comparisons between experimental values and NAAPS modeled sea-salt mass concentrations together with corresponding wind velocities obtained from measurements and the model (middle panel) as well as

measured rain rate and modeled sea-salt wet deposition rate (lower panel).

[36] For the entire experiment, the correlation coefficient for measured and modeled sea-salt mass concentrations is equal to 0.55, the lowest of all experiments considered here (see Table 1). The same tendency for NAAPS overestimation of concentrations is observed. A large disagreement between the model and observations is observed during two events, around day 204 and at the end of the experiment. Both periods are characterized by increased surface winds, compared with the average during the experiment. Thus, we should observe an increase in the sea-salt concentration assuming that particles were not removed by wet deposition. Indeed, this increase is seen in the model predictions, whereas measurements indicate either a decrease or small amplitude increase of the sea-salt concentration. Additionally, these cases were not affected by wet deposition. Rain was observed on day 205 just when winds were becoming calmer. For the entire experiment, average measured concentration is as low as 1.3 μg/m^3 (see also Table 1). These low concentrations suggest that whitecapping, being the main source of the sea spray, did not occur often in the region.

Table 1. Surface Sea-Salt Concentration Statistics From Analyzed PMEL Experiments: Measurements, Model Values, and Correlation Coefficient[a]

Experiment	Measurements Average, $\mu g/m^3$	NAAPS Average, $\mu g/m^3$	Correlation Coefficient: R
Aerosols99	9.3	14.1	0.60
INDOEX	4.9	6.2	0.83
ACE-Asia	5.6	11.1 (10.1)	0.71 (0.75)
NEAQS-2002	1.3	2.8	0.55
NEAQS-2004	1.5	2.4	0.84
All data	4.6	7.3 (7.1)	0.76 (0.79)

[a]The values in parentheses exclude one outlier point.

Many observations of the whitecap ratio, collected by *Lewis and Schwartz* [2004], indicate that there is a threshold value of wind speed for the onset of wave breaking. Suggestions for such threshold value are about ∼3–5 m/s [*Lewis and Schwartz*, 2004] or larger [*Stramska and Petelski*, 2003], depending on other environmental parameters affecting wave breaking. For the Gulf of Maine, because of the proximity of land and limited wind fetch, the wind speed threshold may be on its higher end. In this case, sea-salt emissions would be lower than predicted assuming no threshold. Analyzing Figure 4 from this perspective, we conclude that periods of winds stronger than the threshold for whitecapping might not have been long enough to sustain higher background sea-salt concentrations and to raise sea-salt mass concentration to local production-deposition equilibrium.

4.4. NEAQS-ITCT 2004 Experiment

[37] The NEAQS-Intercontinental Transport and Chemical Transformation (ITCT) project was conducted between 5 July and 12 August of 2004. The study was the continuation of the NEAQS-2002 project with the focus on air quality along the Eastern Seaboard and transport of North American emissions into the North Atlantic. The Gulf of Maine was again the operational field for NOAA research vessel Ronald H. Brown, deployed with the PMEL instrumentation performing aerosol chemical measurements near the surface. Figure 5 presents the comparisons between measured and modeled sea-salt mass concentrations (top panel). Accompanying surface wind velocities are plotted in the middle panel, and the bottom panel presents measured rain rate and modeled sea-salt wet deposition rate during the cruise.

[38] A high correlation coefficient, equal to 0.84, is observed between modeled and measured values for the
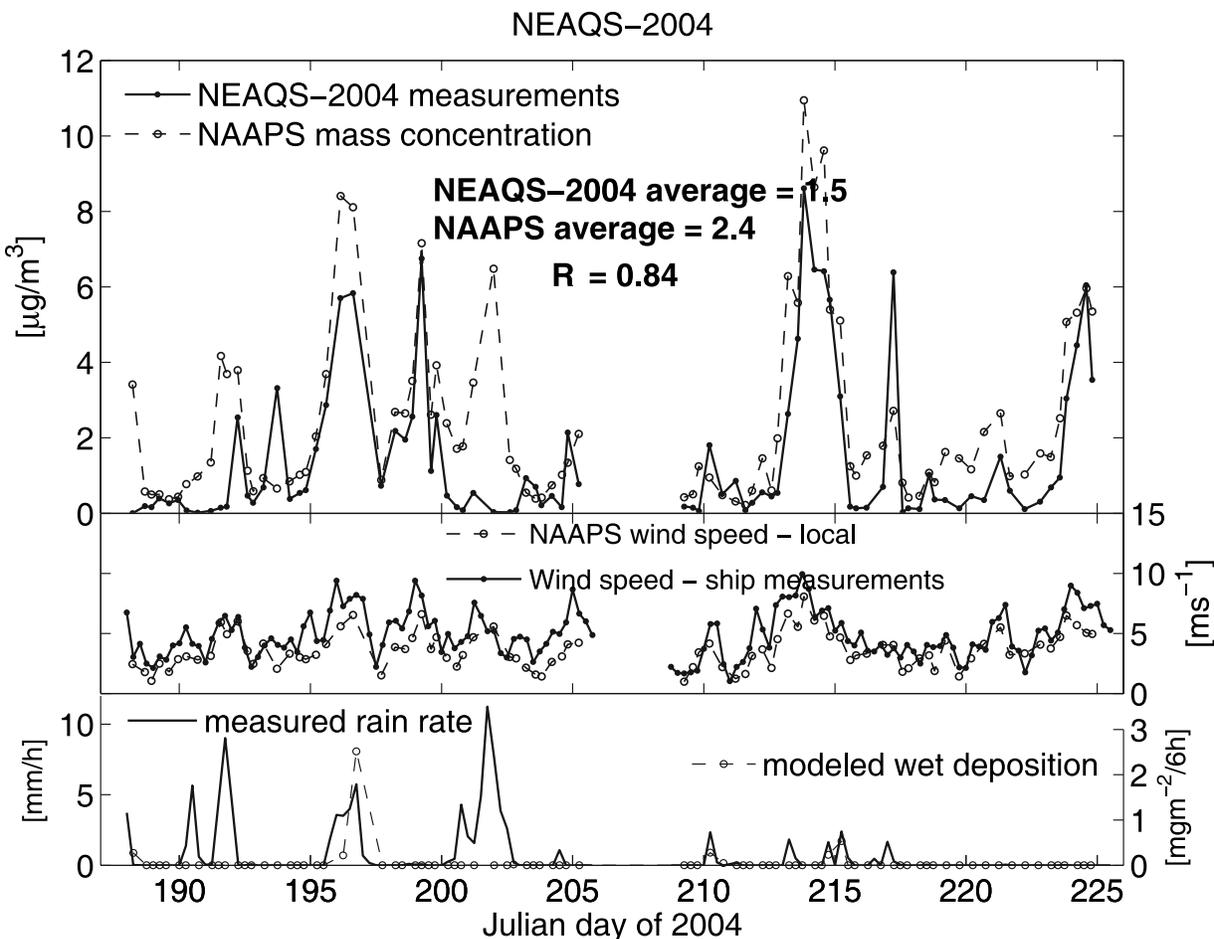
Figure 5. Top panel, comparison of the model concentrations with the measurements during the NEAQS-2004 experiment; middle panel, measured and NAAPS-modeled wind speed during the cruise; lower panel, rain rate measured from the ship (left axis) and rate of sea-salt wet deposition in the model (right axis).
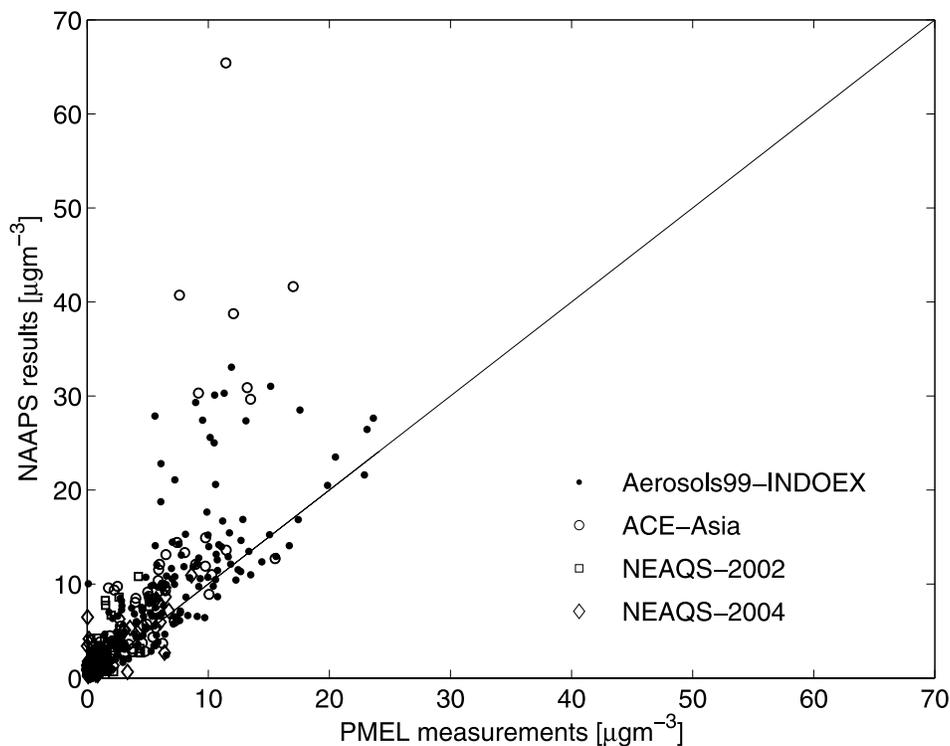
Figure 6. Measured versus modeled sea-salt concentrations based on four PMEL experiments (359 data points. Solid circles represent Aerosols99-INDOEX, open circles represent ACE-Asia, open squares represent NEAQS-2002, and open diamonds represent NEAQS-2004 data.

total of 86 comparison points. The average modeled sea-salt mass concentration is higher than the average of the observations, but the amplitude of peak concentrations during specific events is often well preserved by NAAPS. Additionally, some disagreements between the two data sets may be explained by rainfall occurrences, which were not resolved in the model. These include the first data point, higher modeled loading around day 192, and the event between days 200 and 203. These cases are good examples of how rain events may have suppressed the measured sea-salt loading and lead to discrepancy between the model and observations. The opposite trend is observed around days 194 and 217, where observations show temporary sharp increases in the sea-salt mass, exceeding modeled values. Despite no wind speed increase during these days and small rainfall observed prior to the second episode, observations indicate larger concentrations. We do not have a good explanation for this case.

5. Comparison With Experimental Data: Discussion

[39] Figure 6 shows a scatterplot for measured and modeled sea-salt mass concentrations based on all discussed experiments. The overall correlation coefficient is 0.76 and, excluding one outlier, it is 0.79. All statistics, including the average measured and modeled values from investigated PMEL experiments, together with corresponding correlation coefficients, are presented in Table 1. The values in parentheses in Table 1 exclude one outlier point. The average measured sea-salt mass concentration is 4.6 $\mu g/m^3$ while

that derived from NAAPS equals 7.3 $\mu g/m^3$. For concentrations higher than about 5 $\mu g/m^3$, deviations are substantial (see Figure 6), with NAAPS generally overestimating measured mass.

[40] One possible reason for the disagreement is the representation of wet removal processes because of problems with moist thermodynamics in the global weather forecast model. To investigate the role of precipitation, we excluded measurements affected by rainfalls from some comparisons.

[41] In particular, Figure 7 presents the correlation coefficient (solid line, left axis) together with the slope (dashed line, right axis) between measured and modeled sea-salt concentrations as a function of rain rate cumulative count (one outlier was omitted in the analysis).

[42] Out of 358 data points, 252 are free of precipitation. The correlation coefficient for this data set increased from 0.79 to 0.87 for cases with no precipitation. This result demonstrates the impact of storm activity on model accuracy. The relationship between modeled and measured sea-salt concentrations is closer to 1:1 for dry cases (left side of the dashed line in Figure 7). For all data points, this relationship is approximately 1:1.3, mostly because of the model overestimations during the ACE-Asia and the Aerosols99 experiments.

[43] As we suggested previously (ACE-Asia results), the discrepancies between the model and measurements might vary depending on surface wind conditions. In Figure 8, the difference between measured and modeled sea-salt mass is plotted as a function of the local wind speed for points without precipitation. Indeed, for stronger winds, larger
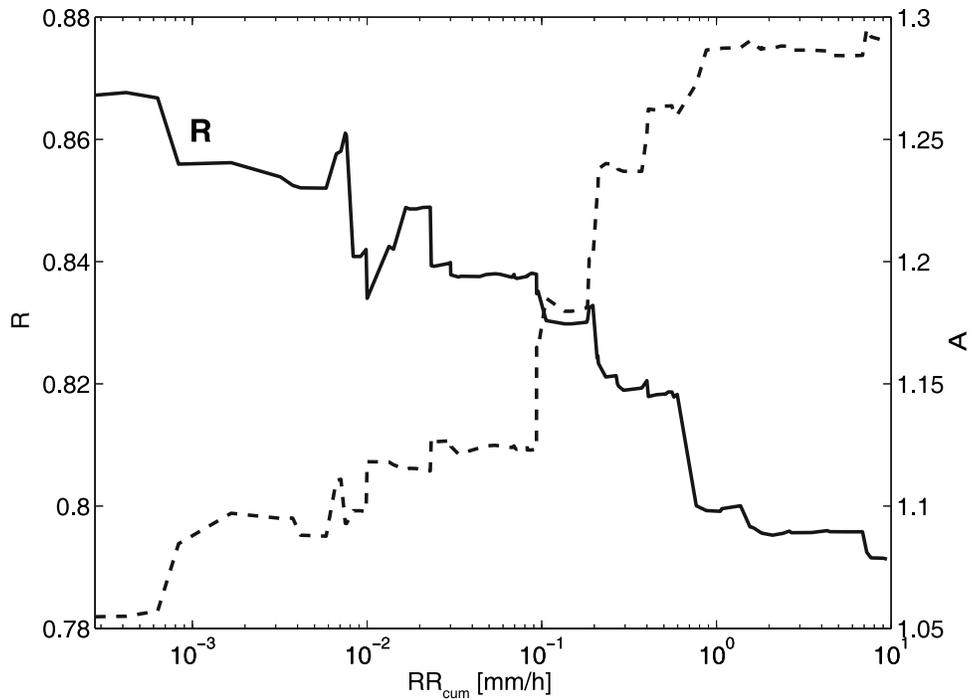
Figure 7. Modeled versus measured sea-salt concentration correlation coefficient R (left axis) and linear fit slope rate A (right axis), according to the equation $CONC_{model} = A*CONC_{PMEL} + B$, as a function of rain rate cumulative count RR_{cum}. The lowest value of rain rate represent the situation when all observations with precipitation were excluded in the computation, whereas the highest rain rate stands for the situation where all points were included in the computations. One outlier point was omitted in analysis.
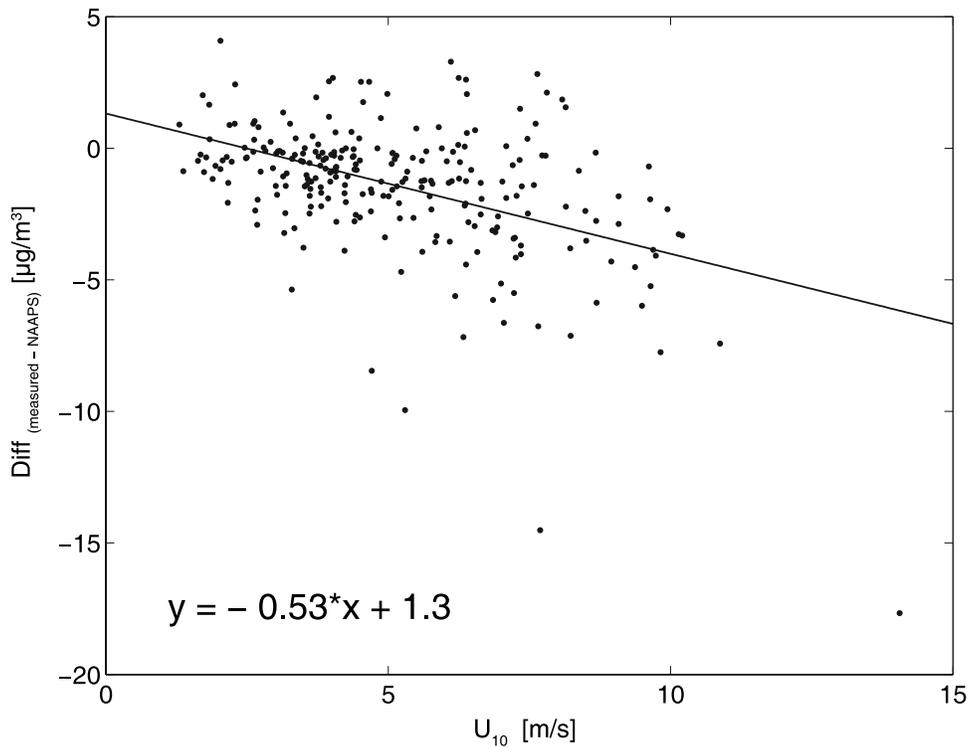
Figure 8. Difference Diff between measured and modeled sea-salt mass concentration as a function of surface wind velocity U_{10}. Only points without precipitation influence are considered. Solid line represents linear fit to the data.

Table 2. Surface Wind Speed Statistics From Analyzed PMEL Experiments: Measurements, Model Values, and Correlation Coefficient[a]

Experiment	Measurements Average, m/s	NAAPS Average, m/s	Correlation Coefficient: R
Aerosols99	6.6 (6.6)	7.1 (6.7)	0.69 (0.6)
INDOEX	5.0 (4.8)	5.0 (4.8)	0.79 (0.84)
ACE-Asia	6.9 (5.4)	6.9 (5.3)	0.88 (0.86)
NEAQS-2002	5.1 (5.0)	4.4 (4.3)	0.69 (0.62)
NEAQS-2004	4.8 (4.5)	3.6 (3.4)	0.83 (0.82)
All data	5.6 (5.1)	5.3 (4.8)	0.81 (0.80)

[a]The values in parentheses are for data points without precipitations.

differences are observed, although there is large scatter in the data. Negative values, indicating NAAPS overpredictions, dominate for the stronger wind speed regime.

[44] One possible mechanism for such a trend was already mentioned when results from the ACE-Asia experiment were discussed. It is the strong nonlinearity of the source function versus surface wind speed (power law with exponent of 3.41), which might lead to emission overestimation for higher wind speed regimes [*Andreas*, 1998]. However, this trend can also be associated with systematic errors related to the method by which dry deposition is handled in the model. Because of the lack of deposition velocity differentiation for different particle sizes, a systematic excess of mass can be modeled. For stronger wind speeds, with larger sea-salt loading, this systematic error may become substantial and dominate among factors determining discrepancies. Systematic study of this effect is needed to assess its magnitude and to improve the model.

[45] Table 2 summarizes the statistics of observed and modeled wind speed during all analyzed experiments. The values in the parentheses reflect similar statistics but with precipitation cases excluded from the analysis. The total average is slightly higher for measurements than for the model, mostly due to underestimated NOGAPS wind velocities during the two NEAQS experiments. Model agreement with observations is good; correlation varies from 0.69 to 0.83 depending on the project, with an average value of 0.81.

[46] Two interesting facts can be inferred when statistics from Table 2 are analyzed together with average sea-salt values from measurements.

[47] First, we can see that the ACE-Asia average wind speed is higher than during Aerosols99. However, the average sea-salt mass concentration is lower (5.6 versus 9.28 μg/m^3), which is contradictory to expectations. Most likely, this is because during the Aerosols99, the ship cruised almost all the time in the open ocean, whereas during ACE-Asia, it spent some time on the calmer Japan Sea and closer to the shore where wave characteristics are affected by the proximity of land [*Stramska and Petelski*, 2003]. Other factors like the difference in the rain rate could also be important, but on average, more rain was observed during Aerosols99 than during ACE-Asia. It is also important that very strong wind speed episodes during the ACE-Asia experiment, sometimes exceeding 15 m/s, were not reflected in high sea-salt loadings. Measured sea-salt mass concentration never exceeded 20 μg/m^3. An analogous situation is observed in the case of the two NEAQS projects. The average sea-salt mass concentration for NEAQS-2002

and NEAQS-2004 are very similar (1.3 and 1.5 μg/m^3, respectively, see also Table 1), despite the fact that on average, wind speed was stronger during NEAQS-2002 (see Table 2).

[48] Secondly, it is interesting to compare the NEAQS projects with the INDOEX experiment. During INDOEX, the average wind velocity was 5.0 m/s, similar to those observed during NEAQS experiments. However, sea-salt measurements during INDOEX indicate much higher concentrations, with an average (4.9 μg/m^3) being a factor of 3−4 larger than NEAQS averages. Wet deposition cannot account for low NEAQS values. It is also not likely that the dry deposition was substantially different in both regions to produce such variation in surface concentrations. It is evident from this example that besides wind speed, there are other factors influencing the sea-salt surface concentrations. The proximity of a large continent and the importance of advection from the source free direction can be an important issue, as indicated by *Lewis and Schwartz* [2004]. *Reid et al.* [2001] concluded that during offshore winds, a steady state vertical distribution of sea-salt particles was achieved at a distance of ∼35−50 km from the shore, depending on the wind speed. Therefore we investigated measurements from both NEAQS projects to determine if they exhibit any relation on the average wind direction. We divided the measurements into two advection categories, (1) offshore, advection from the land, defined by angels between 250→20; and (2) onshore, advection from the ocean, defined by angels between 70→200. Table 3 presents statistics from performed analysis. Only measurements without precipitation are considered. For both NEAQS experiments, the average sea-salt mass concentration measured during the onshore advection is higher than during the offshore winds, 1.55 versus 0.85 μg/m^3 in the case of NEAQS-2002 and 1.89 versus 0.60 μg/m^3 in the case of NEAQS-2004. These results seem to indicate that the sea-salt surface concentrations measured during the experiments were sometimes influenced by the vicinity of land. However, stronger winds from the onshore direction, as indicated in Table 3, can account for the differences in some part. This is especially apparent in the case of NEAQS-2004, where the difference between average wind speeds from both directions is 1.2 m/s. Therefore additional study needs to be performed to explain quantitatively the influence of land on the sea-salt surface concentrations, even as far as tens or hundreds kilometers from shore.

[49] The other aspects that can be of importance when comparing the INDOEX and NEAQS averages are potential weaknesses of the assumed source function, as well as possible variability in the whitecapping and emission in both regions. We already suggested the possible importance of threshold wind speed for the onset of wave breaking. The problem with this parameter is that it is not precisely determined by wind speed alone. *Stramska and Petelski* [2003] noticed that the overall degree of whitecapping is determined by a combination of various conditions characterizing both wind and wavefield. Therefore the onset of wave breaking cannot be reduced to a single parameter dependency. Stramska and Petelski have also shown that wave breaking depends on the duration of wind action, which is related to the sea state development. They observed more whitecaps under developed seas than under

Table 3. Statistics From NEAQS-2002 and NEAQS-2004 Experiments Computed for Offshore and Onshore Average Wind Directions and for the Total Experiment Period[a]

	NEAQS-2002			NEAQS-2004		
	Average Concentration, $\mu g/m^3$	Average Wind Speed, m/s	Number of Observations	Average Concentration, $\mu g/m^3$	Average Wind Speed, m/s	Number of Observations
Offshore	1.55	4.8	15	1.89	5.1	20
Onshore	0.85	4.7	10	0.60	3.9	17
Total	1.21	5.0	40	1.31	4.5	55

[a]On-shore direction is defined by angles between 70 and 200 degrees, whereas off-shore direction is defined by angles between 250 and 20 degrees, clockwise. Measurements without precipitation are only considered.

rising seas or under decreasing wind conditions. They also suggested that local conditions and regional sea state characteristics influence wave-breaking probability and in result, sea-salt emission. *Zhao and Toba* [2001], on the other hand, showed that whitecap ratio is better described by the nondimensional breaking-wave parameter, defined as the square friction velocity divided by the peak wave angular frequency and kinematic viscosity of air. These and other studies [*Hanson and Phillips*, 1999; *Xu et. al.*, 2000; *Petelski et al.*, 2005] may suggest the need to incorporate parameters other than wind speed to improve wave breaking and sea-salt emission parameterization. Our findings also support this necessity.

[50] Other parameters identified to have a potential influence on the process of the sea-salt aerosol production are the sea surface temperature T_w and the water salinity S [*Monahan and O'Muircheartaigh*, 1980; *Lewis and Schwartz*, 2004; *Stramska and Petelski*, 2003]. The recent study of *Mårtensson et al.* [2003] shows the dependence of the sea-salt aerosol emission, originating from bursting air bubbles at the water's surface, on the water salinity and temperature. Consequently, the sea-salt mass flux should be larger for higher salinities and warmer seawaters. These laboratory results have not yet been tested in the open-ocean observations, although several attempts were made to investigate the relationship [*Bortkovskii*, 1987; *Wu*, 1988; *Stramska and Petelski*, 2003]. We analyzed the data to examine the temperature dependence on the surface sea-salt aerosol mass loadings. The effect of salinity is not considered here because of the small span of salinities, in the range between 30 and 37‰.

[51] In Figure 9, the difference between measured and modeled sea-salt mass concentration is plotted as a function of the sea surface temperature. Only points without precipitations are considered. If there was a relation between the measured sea-salt mass concentration and water temperature, some trend should be observed on Figure 9, because the model results do not account for such dependency. We
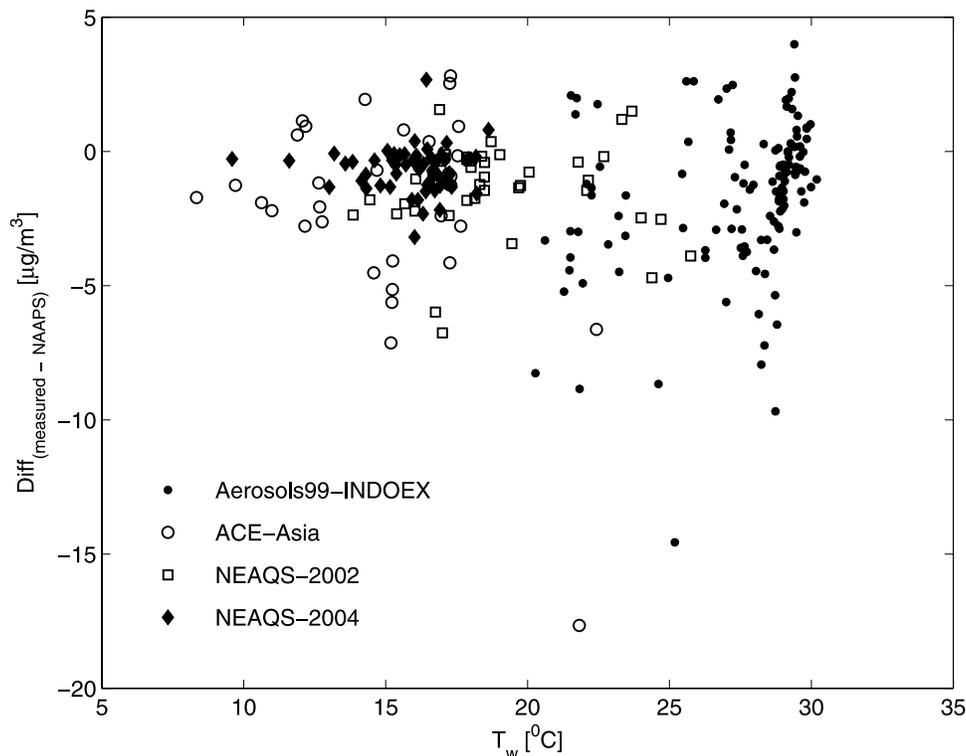
Figure 9. Difference Diff between measured and modeled sea-salt mass concentration as a function of the water temperature T_w. Only points without precipitation influence are considered.

fail to observe any trend in our data set. This indicates that the sea-salt aerosol emission dependence on a seawater temperature cannot be concluded from our analysis. If such dependence exists, more sophisticated measurements and model simulations are needed to depict it.

6. Summary

[52] In this study, we used open-ocean measurements of the sea-salt mass concentrations from five different campaigns, spread in time and space. This data set is from shipboard observations, free from typical problems associated with the impact of surf zone on land stations measurements. To investigate the validity of the sea-salt parameterizations, we employed a global forecasting model and a transport model with detailed representation of dry and wet deposition, advection and diffusion, and other physical processes. We show that the inclusion of these processes leads to good agreement with shipboard measurements. The model's ability to predict surface sea-salt mass concentration, measured by the correlation coefficient, varied from 0.55 in the case of NEAQS-2002 to 0.84 during the NEAQS-2004 experiment. Combining all experiments, 359 data points were available for validation. For the combined data set, we obtained a correlation coefficient of 0.76. When 106 cases influenced by precipitation were excluded from the analysis, we obtained a correlation coefficient of 0.87. Apart from wet deposition uncertainties, model-measurement discrepancies were found to be influenced by uncertainties in emissions at high wind speeds. Other suggested factors affecting comparisons were lack of a wind speed threshold for the emission onset and lack of size differentiation for deposition velocity. Some of these aspects, like wet deposition, were proved to substantially reduce the model's accuracy. On the other hand, the water temperature changes showed no discernible effect on measured sea-salt concentrations and performed comparisons. The impact of other factors requires further studies to determine their significance and magnitude.

References

Andreas, E. L. (1998), A new sea spray generation function for wind speeds up to 32 ms^{-1}, *J. Phys. Oceanogr.*, *28*, 2175–2184.
Bates, T. S., P. K. Quinn, D. J. Coffman, J. E. Johnson, T. L. Miller, D. S. Covert, A. Wiedensohler, S. Leinert, A. Nowak, and C. Neususs (2001), Regional physical and chemical properties of the marine boundary layer aerosol across the Atlantic during Aerosols99: An overview, *J. Geophys. Res.*, *106*(D18), 20,767–20,782, doi:10.1029/2000JD900578.
Bates, T. S., D. J. Coffman, D. S. Covert, and P. K. Quinn (2002), Regional marine boundary layer aerosol size distributions in the Indian, Atlantic, and Pacific Oceans: A comparison of INDOEX measurements with ACE-1, ACE-2, and Aerosols99, *J. Geophys. Res.*, *107*(D19), 8026, doi:10.1029/2001JD001174.
Berner, A., C. Lurzer, F. Pohl, O. Preining, and P. Wagner (1979), The size distribution of the urban aerosol in Vienna, *Sci. Total Environ.*, *13*, 245–261.
Bortkovskii, R. S. (1987), *Air-Sea Exchange of Heat and Moisture During Storms*, pp. 1–124, Springer, New York.
Christensen, J. H. (1997), The Danish eulerian hemispheric model—A three-dimensional air pollution model used for the arctic, *Atmos. Environ.*, *31*, 4169–4191.
Gong, S. L. (2003), A parameterization of sea-salt aerosol source function for sub- and super-micron particles, *Global Biogeochem. Cycles*, *17*(4), 1097, doi:10.1029/2003GB002079.
Gong, S. L., L. A. Barrie, and M. Lazare (2002), Canadian Aerosol Module (CAM): A size-segregated simulation of atmospheric aerosol processes for climate and air quality models. 2. Global sea-salt aerosol and its budgets, *J. Geophys. Res.*, *107*(D24), 4779, doi:10.1029/2001JD002004.
Grini, A., G. Myhre, J. K. Sundet, and I. S. A. Isaksen (2002), Modeling the annual cycle of sea salt in the global 3D model Oslo CTM2: Concentrations, fluxes, and radiative impact, *J. Clim.*, 1717–1730.
Gryning, S. E., and E. Batchvarova (1990), Analytical model for the growth of the coastal internal boundary layer during onshore flow, *Q. J. R. Meteorol. Soc.*, *116*, 187–203.
Guelle, W., M. Schulz, and Y. Balkanski (2001), Influence of the source formulation on modeling the atmospheric global distribution of sea salt aerosol, *J. Geophys. Res.*, *106*, 27,509–27,524.
Hanson, J. L., and O. M. Phillips (1999), Wind sea growth and dissipation in the open ocean, *J. Phys. Oceanogr.*, *29*, 1633–1648.
Hertel, O., J. Christensen, E. Runge, W. A. H. Asman, R. Berkowicz, M. Hovmand, and O. Hov (1995), Development and testing of a new variable scale air pollution model—ACDEP, *Atmos. Environ.*, *29*, 1267–1290.
Hogan, T. F., and T. E. Rosmond (1991), The description of the Navy Operational Global Atmospheric Prediction Systems Spectral Forecast Model, *Mon. Weather Rev.*, *119*, 1786–1815.
Holland, H.D. (1978), *The Chemistry of the Atmosphere and Oceans*, p. 154, John Wiley, Hoboken, N. J.
Hoppel, W. A., G. M. Frick, and J. W. Fitzgerald (2002), Surface source function for sea-salt aerosol and aerosol dry deposition to the ocean surface, *J. Geophys. Res.*, *107*(D19), 4382, doi:10.1029/2001JD002014.
Inversen, T. (1989), Numerical modelling of the long range atmospheric transport of sulphur dioxide and particulate sulphate to the arctic, *Atmos. Environ.*, *23*, 2571–2595.
Lewis, E. R., and S. E. Schwartz (2004), *Sea Salt Aerosol Production: Mechanisms, Methods, Measurements and Models: A Critical Review, Geophysical Monograph*, 152, AGU, Washington, D. C.
Mårtensson, E. M., E. D. Nilsson, G. de Leeuw, L. H. Cohen, and H. C. Hansson (2003), Laboratory simulations and parameterization of the primary marine aerosol production, *J. Geophys. Res.*, *108*(D9), 4297, doi:10.1029/2002JD002263.
Monahan, E. C., and I. O'Muircheartaigh (1980), Optimal power-law description of oceanic whitecap coverage dependence on wind speed, *J. Phys. Oceanogr.*, *10*, 2094–2099.
Monahan, E. C., D. E. Spiel, and K. L. Davidson (1986), A model of marine aerosol generation via whitecaps and wave disruption, in *Oceanic Whitecaps and Their Role in Air-Sea Exchange Processes*, edited by E.C. Monahan and G. MacNiocaill, pp. 167–174, Springer, New York.
Park, P. M., M. H. Smith, and H. J. Exton (1990), The effect of mixing height on maritime aerosol concentrations over the North Atlantic Ocean, *Q. J. R. Meteorol. Soc.*, *116*, 461–476.
Petelski, T., J. Piskozub, and B. Paplinska-Swerpel (2005), Sea spray emission from the surface of the open Baltic Sea, *J. Geophys. Res.*, *110*, C10023, doi:10.1029/2004JC002800.
Quinn, P. K., D. J. Coffman, V. N. Kapustin, T. S. Bates, and D. S. Covert (1998), Aerosol optical properties in the marine boundary layer during ACE 1 and the underlying chemical and physical aerosol properties, *J. Geophys. Res.*, *103*, 16,547–16,563.
Quinn, P. K., D. J. Coffman, T. S. Bates, T. L. Miller, J. E. Johnson, K. Voss, E. J. Welton, and C. Neususs (2001), Dominant aerosol chemical components and their contribution to extinction during the Aerosols99 cruise across the Atlantic, *J. Geophys. Res.*, *106*, 20,783–20,809.
Quinn, P. K., D. J. Coffman, T. S. Bates, T. L. Miller, J. E. Johnson, E. J. Welton, C. Neususs, M. Miller, and P. J. Sheridan (2002), Aerosol optical properties during INDOEX 1999: Means, variability and controlling factors, *J. Geophys. Res.*, *107*(D18), 8020, doi:10.1029/2000JD000037.
Reid, J. S., H. H. Jonsson, M. H. Smith, and A. Smirnov (2001), Evolution of the vertical profile and flux of large sea-salt particles in a coastal zone, *J. Geophys. Res.*, *106*, 12,039–12,053.
Ritchie, H. (1987), Semi-Lagrangian advection on a Gaussian grid, *Mon. Weather Rev.*, *115*, 608–619.
Slinn, A. A., and W. G. Slinn (1980), Predictions for particle deposition on natural waters, *Atmos. Environ.*, *14*, 1013–1016.
Smith, M. H., P. M. Park, and I. E. Consterdine (1993), Marine aerosol concentrations and estimated fluxes over the ocean, *Q. J. R. Meteorol. Soc.*, *119*, 809–824.

Staniforth, A., and J. Cote (1991), Semi-Lagrangian integration schemes for atmospheric models—A review, *Mon. Weather Rev.*, *119*, 2206–2223.

Stramska, M., and T. Petelski (2003), Observations of oceanic whitecaps in the north polar waters of the Atlantic, *J. Geophys. Res.*, *108*(C3), 3086, doi:10.1029/2002JC001321.

Takemura, T., H. Okamoto, Y. Maruyama, A. Numaguti, A. Higurashi, and T. Nakajima (2000), Global three-dimensional simulation of aerosol optical thickness distribution of various origins, *J. Geophys. Res.*, *105*, 17,853–17,873.

Walcek, C. J., R. A. Brost, J. S. Chang, and M. L. Wesely (1986), SO$_2$, sulfate and HNO$_3$ deposition velocities computed using regional landuse and meteorological data, *Atmos. Environ.*, *20*, 949–964.

Wu, J. (1988), Variations in whitecap coverage with wind stress and water temperature, *J. Phys. Oceanogr.*, *18*, 1448–1453.

Xu, D., X. Liu, and D. Yu (2000), Probability of wave breaking and whitecap coverage in a fetch-limited sea, *J. Geophys. Res.*, *105*, 14,253–14,259.

Zhao, D., and Y. Toba (2001), Dependence of whitecap coverage on wind and wind-wave properties, *J. Oceanogr.*, *57*, 603–616.

————————

P. J. Flatau, Scripps Institution of Oceanography, University of California, San Diego, La Jolla, CA 92093, USA.

P. K. Quinn, Pacific Marine Environmental Laboratory, National Oceanic & Atmospheric Administration, 7600 Sand Point Way NE, Seattle, WA 98115, USA.

D. L. Westphal, Marine Meteorology Division, Naval Research Laboratory, 7 Grace Hopper Ave., Monterey, CA 93943, USA.

M. L. Witek, Interdisciplinary Centre of Mathematical and Computational Modeling, University of Warsaw, ul. Pawiñskiego 5a, 02-106, Warsaw, Poland. (mwit@igf.fuw.edu.pl)